Ionics (2015) 21:1605–1613
DOI 10.1007/s11581-014-1341-7

ORIGINAL PAPER

Spectroscopic and computational analysis of the molecular interactions in the ionic liquid $[Emim]^+[FAP]^-$

James X. Mao · Krishnan Damodaran

Received: 11 September 2014 / Revised: 25 November 2014 / Accepted: 2 December 2014 / Published online: 20 December 2014

Abstract A weakly coordinating room-temperature ionic liquid, 1-ethyl-3-methyl imidazolium tris(pentafluoroethyl)-trifluorophosphate ($[Emim]^+[FAP]^-$), is investigated by DFT method at B3LYP/6-31+G(d, p) level. Four locally stable conformers of the ion pair were located. Atoms-in-molecules (AIM) and electron density analysis indicated the existence of hydrogen bonds. Further investigation through Natural Bond Orbital (NBO) analysis provided insight into the origin for weaker ion pair interactions. Harmonic vibrations of the ion pair were calculated and compared with the experimental Raman and infrared spectra. Assignments and frequency shifts are discussed in light of the inter-ionic interactions.

Keywords Ionic liquid · DFT · Raman · Infrared

Introduction

Room-temperature ionic liquids (RTILs) have gained a wide variety of attentions and applications in recent years [1]. They are salts with a bulky and asymmetric organic cation, which inhibits an ordered crystalline structure to form, and have low melting points (melting points below 100 °C). RTILs posses very low vapor pressure and are nonflammable, which provide an environmentally friendly alternative to organic solvents [2–5]. They have great potential applications in CO_2 removal process due to its stability and non-volatile nature [6, 7]. Their electrochemical and thermal stability also make them a potential replacement of existing electrolytes for high efficiency electrochemical devices [8, 9].

Hexafluorophosphate ($[PF_6]^-$) based RTILs are a class of most widely used RTILs in many fields. However, $[PF_6]^-$ anion is hydrolytic unstable at high temperature: HF is produced following the reaction between $[PF_6]^-$ anion and water. By introducing hydrophobic pentafluoroethyl groups to replace some fluorine atoms, Ignat'ev and his co-workers [10] synthesized a new RTIL anion: tris(pentafluoroethyl)-trifluorophosphate ($[FAP]^-$). Due to its unique properties, it shows promising applications in many fields since its birth. $[FAP]^-$ based RTILs are hydrolytic stable, and are the most hydrophobic of all RTILs which have been synthesized: their water uptakes are more than 10 times less in comparison with the $[PF_6]^-$ based RTILs [10]. Together with their negligible vapor pressures, $[FAP]^-$ based RTILs were proposed as an ideal extraction solvents in separation processes, especially in the sampling of large volumes of aqueous solutions [11]. Indeed, $[FAP]^-$ based RTILs show much higher selectivity and capacity at infinite dilution than the generally used organic solvents [12]. Due to their hydrolytic stability and low viscosity, they are also very promising in tribological applications: tribological tests showed very low friction coefficient while $[FAP]^-$ based RTILs were used as neat lubricant [13, 14], and the anti-friction and anti-wear performance of the base oil were substantially improved when $[FAP]^-$ based RTILs were used as an additives [15, 16]. They have a very broad electrochemical window, which offers perspectives for increasing the maximum voltage in supercapacitor applications or other electrochemical devices [17]. Computational screening predicted $[FAP]^-$ based RTILs should increase the solubility of CO_2 compared to a wide range of conventional anions, and it was confirmed experimentally: $[FAP]^-$ based RTILs

J. X. Mao · K. Damodaran (✉)
Department of Chemistry, University of Pittsburgh,
15260, Pittsburgh, Pennsylvania
e-mail: damodak@pitt.edu

can absorb more than 70 % more CO_2 relative to PF_6^- based RTILs [18–20].

All these interesting physicochemical properties of $[FAP]^-$ based RTILs, which in turn are governed by the interactions prevailing between their cations and anions [21–23], make $[FAP]^-$ based RTILs a class of very attractive ionic liquids. The growing interests in $[FAP]^-$ based RTILs require better understanding of the mechanism behind all these interesting physical properties. Recently Althuluth et al. [24] studied the gas solubilities in $[Emim]^+[FAP]^-$ using Peng-Robinson Equation of State. As far as we know no other theoretical studies about $[FAP]^-$ based RTILs were reported. In this work, the molecular interactions between the cation $[Emim]^+$ and the anion $[FAP]^-$ was investigated using density functional theory.

Quantum mechanical method

Calculations were performed at Density Functional Theory (DFT) level with the hybrid functional B3LYP, which incorporates Becke's three-parameter exchange functional [25] and the Lee, Yang, and Parr correlation functional [26] using the Gaussian 09 program [27]. The 6-31+G(d, p) basis sets [28] implemented in the Gaussian program were used. The geometries of ion pairs were fully optimized at the B3LYP/6-31+G(d, p) level, and the basis set superposition error (BSSE) [29] was corrected for all interaction calculations using the counterpoise method [30, 31]. Zero-point energies (ZPE) were also corrected for all optimized structures, and frequencies were calculated to ensure that no imaginary components existed. Natural bond orbital (NBO) [32] and atoms in molecules (AIM) [33, 34] analyses were carried out by programs implemented in the Gaussian 09 and Firefly QC package [35] to study the interactions between ion pairs. Vibrational frequencies were assigned by visualizing displacements of atoms around their equilibrium positions and through Potential Energy Distribution (PED) analysis.

Experimental

Chemical

1-Ethyl-3-methylimidazolium tris(pentafluoroethyl)trifluorophosphate (CAS# 377739-43-0) was purchased from EMD Chemicals and used without further purification.

Infrared and raman spectroscopy

The IR spectrum was collected from 400 to 4000 cm^{-1} on an attenuated total reflection (ATR) module with a Nicolet Model 360 FTIR at 2 cm^{-1} nominal resolution. The number of reflections at the diamond crystal surface is "1", and the penetration depth of the system is approximately one-fifth of the wavelength. For the measurement, a droplet of the IL was placed on the ATR crystal under dry nitrogen flow.

Results and discussion

Geometric analysis

Both computational and experimental works [36, 37] showed that the ethyl group bound to the imidazolium ring in $[Emim]^+$ ion is able to rotate to yield different conformers, and there exist two stable $[Emim]^+$ structures: a planar C_s structure and a non-planar C_1 structure (Fig. 1). Umebayashi et al. reported the presence of both conformers in RTIL $[Emim]^+[PF_6]^-$ at a population of 3:2 [37], and our calculations showed the C_1 structure is slightly favored (2.3 kJ/mol) than C_s structure.

In another side, $[FAP]^-$ is reported as a mixture of two isomers: a meridional structure with C_s symmetry and a facial structure with C_3 symmetry (Fig. 2). Our calculations showed that meridional isomer is 7.1 kJ/mol more stable than facial isomer. The meridional isomer is preferably generated in the synthesis reaction but both isomers' coexistence were observed by NMR spectroscopy at a ratio of 85:15 (meridional:facial) [10].

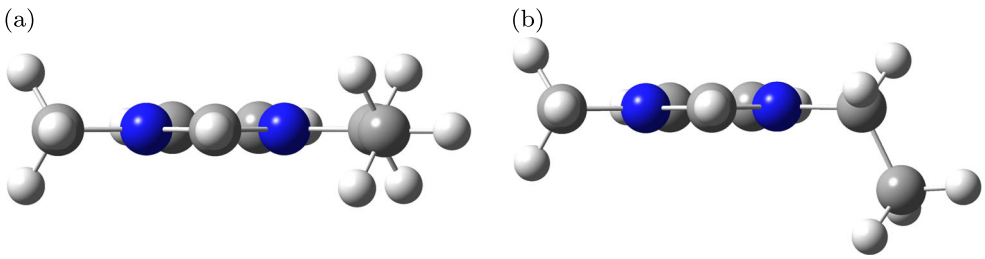

Fig. 1 $[Emim]^+$ cation conformers optimized at the B3LYP/6-31+G** level. (**a**): C_s planar structure. (**b**): C_1 non-planar structure. The non-planar structure is slightly more stable than planar structure by 2.3 kJ/mol

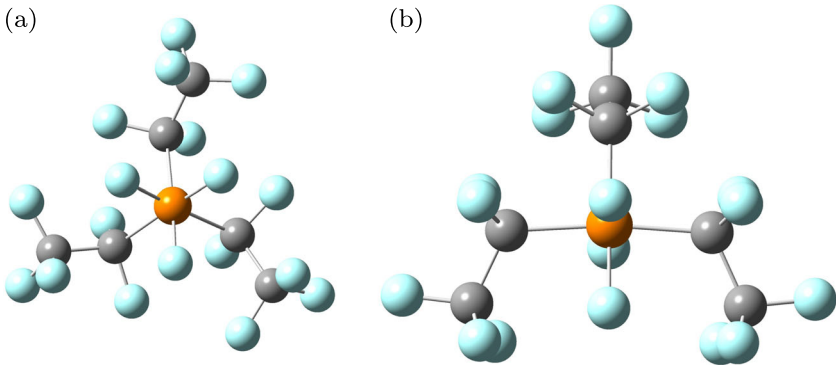

Fig. 2 $[FAP]^-$ anion conformers optimized at the B3LYP/6-31+G** level. (**a**): C_3 facial structure. (**b**): C_s meridional structure. The meridional structure is more stable than facial structure by 7.1 kJ/mol

Due to these small energy difference, it is certainly expected that both of the conformers from cation and anion exist in RTIL $[Emim]^+[FAP]^-$. Both meridional and facial isomer of $[FAP]^-$ anion were placed around planar and non-planar conformer of $[Emim]^+$ cation in various positions to begin geometric optimizations. Four most stable structures of $[Emim]^+[FAP]^-$ ion pair were located during optimization calculations, and they are shown in Fig. 3. These stable geometries were confirmed to be local minima on the potential energy surface through vibrational frequency analysis (no imaginary components). Their energies (E), along with zero-point vibrational energy corrections, are listed in Table 1.

Among the four stable structures (shown in Fig. 3), the only structure in which $[Emim]^+$ takes the C_s planar conformer is structure (d) and it is least stable. Structure (a) and (b) consist of facial $[FAP]^-$ structure and structure (c) and (d) consist of meridional $[FAP]^-$ structure. The energy difference between structures (a) and (c) is almost negligible (1.3 kJ/mol), which means the isomer structure of $[FAP]^-$ ion is not crucial for the stabilization.

AIM analysis

AIM analysis [38] was carried out to identify the interactions between $[Emim]^+$ cation and $[FAP]^-$ anion. In AIM analysis, critical points are identified as the points where all components of the gradient of electron density vanish. They are classified by the number and sign of eigenvalues from the Hessian matrix of molecular electron density at the point. A bond critical point is a critical point with three non-zero eigenvalues and exactly one of them is negative.

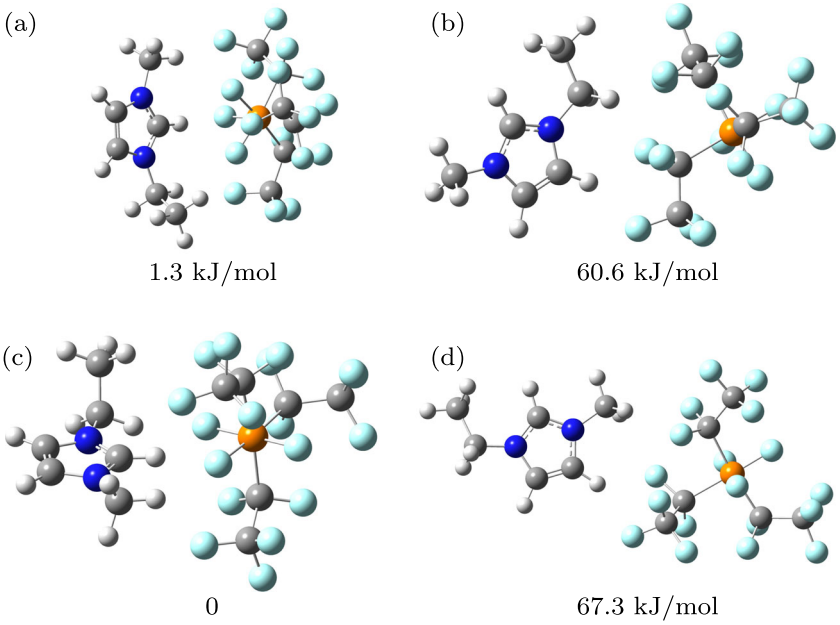

Fig. 3 Optimized stable $[Emim]^+[FAP]^-$ ion pair structures. Relative energy in kJ/mol. $[FAP]^-$ is facial in structures (**a**) and (**b**), and meridional in structures (**c**) and (**d**); $[Emim]^+$ is planar conformer in structure (**d**), and non-planar in structures (**a**), (**b**), and (**c**)

Table 1 Energies[a], energies with ZPE corrections, interaction energies[a], Natural Energy Decompositon Analysis (NEDA), and dispersion interactions for different $[Emim]^+[FAP]^-$ conformations

Structure	E	E+ZPE	E(int)	Natural Energy Decomposition			Dispersion
				Charge Transfer	Electrical	Core	
a	1.3	1.86	288.4	105.0	367.9	-180.1	17.6
b	64.0	63.7	220.9	69.1	271.2	-117.5	16.7
c	0	0	282.6	106.1	357.8	-177.3	19.7
d	67.3	66.98	224.8	65.1	272.6	-112.3	18.3
$[Emim]^+[PF_6]^-$			328.5	94.6	410.6	-176.7	

[a] Relative energies in unit of kJ/mol. [b] Where BSSE correction is considered

An electron density at the bond critical point in the range of 0.002-0.035 has been proposed as a criterion to confirm and characterize existence of a hydrogen bond [33, 34].

For the most stable $[Emim]^+[FAP]^-$ structures (a) and (c) (Fig. 3), eight and seven inter-ionic bond critical points were identified respectively by AIM analysis and electron densities at these located bond critical points were shown in Figs. 4 and 5. The electron densities at these points are all in range of 0.002-0.023, which confirm the existence of hydrogen bondings. For both structures (a) and (c), the strongest hydrogen bondings exist between the F atoms of $[FAP]^-$ and H atom which bonded to C(2) of $[Emim]^+$ (atomic numbering refers to Figs. 6 and 7). Structures (a) and (c) are much more stable than structures (b) and (d) (Fig. 3) because of short distances between $[FAP]^-$ anion and C(2)-H of $[Emim]^+$ cation.

Inter-ionic interactions induce the electron density reorganization between cations and anions. The reorganization can be presented by plotting the difference in electron density ($\Delta\rho = \rho_{\text{ion pair}} - \rho_{\text{cation}} - \rho_{\text{anion}}$) map. The difference electron density maps for the most stable $[Emim]^+$ $[FAP]^-$ conformations were plotted in Figs. 6 and 7. The purple region shows where electron density is enhanced, and the turquoise region is where electron density is depleted. Note that bonds in the region where electron density is enhanced are strengthened, and bonds in the region where electron

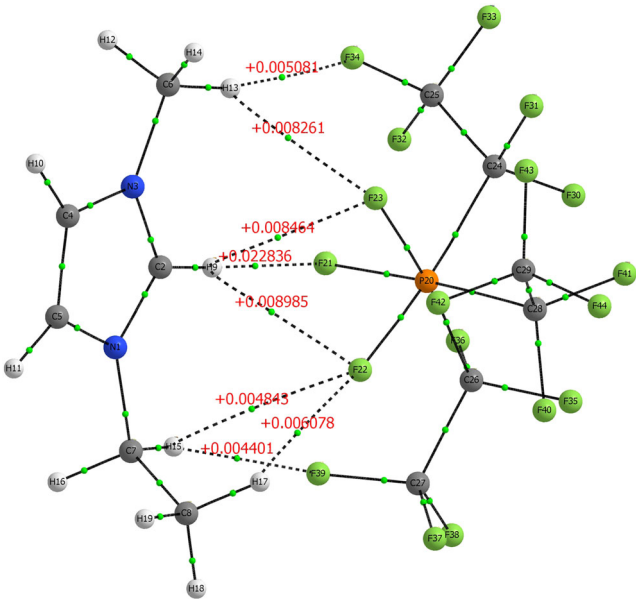

Fig. 4 $[Emim]^+ \cdots [FAP]^-$ inter-ionic hydrogen bonding for structure (**a**). Critical bond points are marked by green points, and electron densities at inter-ionic critical bond points are shown aside

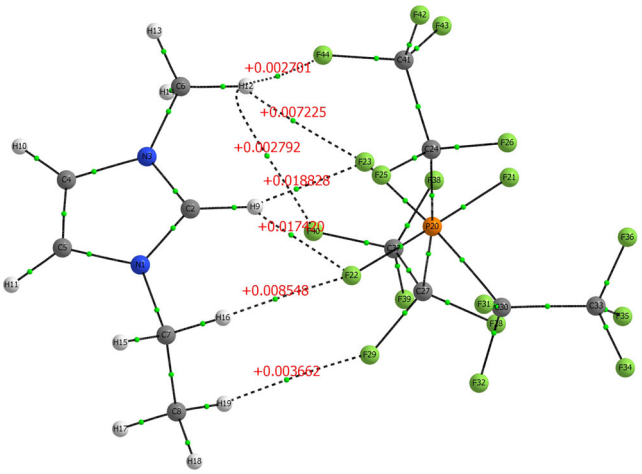

Fig. 5 $[Emim]^+ \cdots [FAP]^-$ inter-ionic hydrogen bonding for structure (**c**). Critical bond points are marked by green points, and electron densities at inter-ionic critical bond points are shown aside

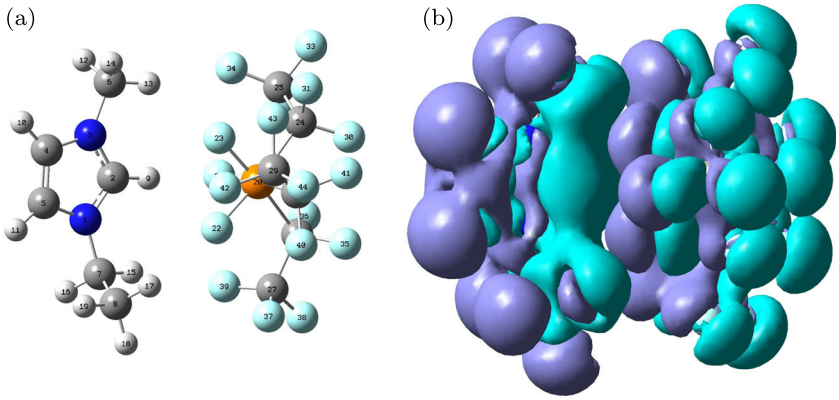

Fig. 6 (**a**): Atom numbering scheme of most stable $[Emim]^+[FAP]^-$ ion pair conformation with facial $[FAP]^-$ structure. (**b**) Corresponding difference electron density ($\Delta\rho = \rho_{\text{ion pair}} - \rho_{\text{cation}} - \rho_{\text{anion}}$) map. Purple region is where $\Delta\rho > 0$ and turquoise region is where $\Delta\rho < 0$

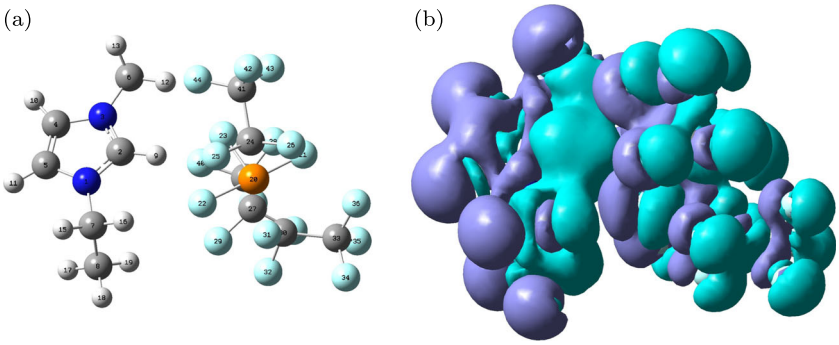

Fig. 7 (**a**): Atom numbering scheme of most stable $[Emim]^+[FAP]^-$ ion pair conformation with meridional $[FAP]^-$ structure. (**b**) Corresponding difference electron density ($\Delta\rho = \rho_{\text{ion pair}} - \rho_{\text{cation}} - \rho_{\text{anion}}$) map. Purple region is where $\Delta\rho > 0$ and turquoise region is where $\Delta\rho < 0$

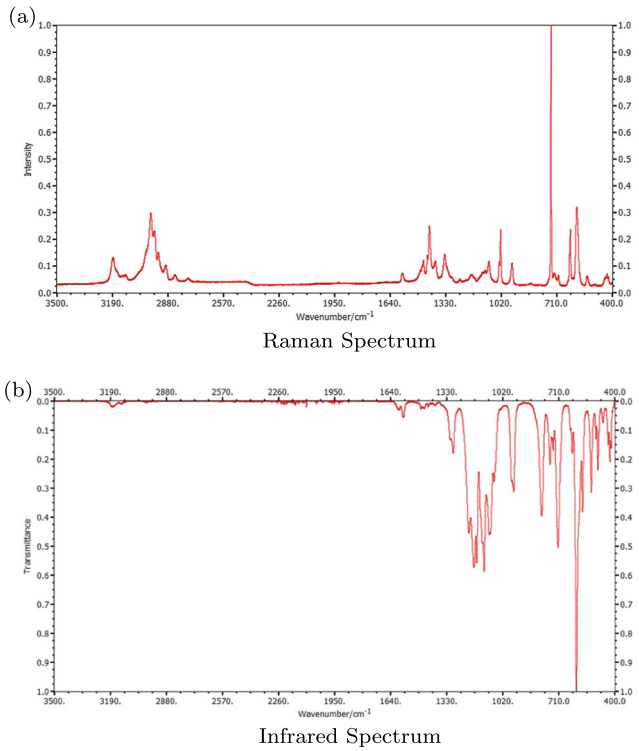

Fig. 8 Raman and IR spectra of $[Emim]^+[FAP]^-$. Range from 400 cm^{-1} to 3500 cm^{-1}

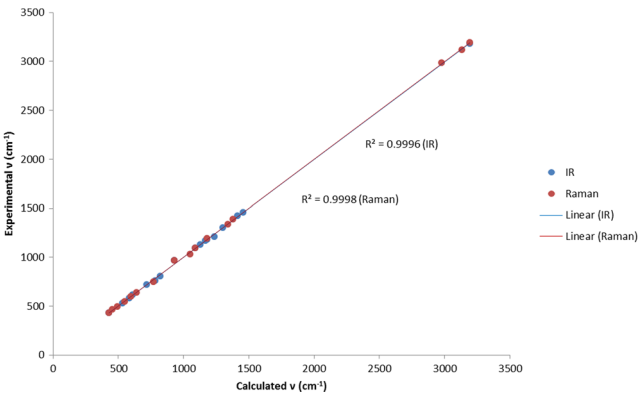

Fig. 9 Correlation diagram for the experimental vibrational spectrum of $[Emim]^+[FAP]^-$ versus calculated frequencies at B3LYP/6-31+G(d,p) level with a scaling factor of 0.964. The correlation coefficient is 0.9996 for IR and 0.9998 for Raman

Table 2 Vibrational assignments of experimental and computed IR and Raman spectra of $[Emim]^+[FAP]^{-}$.[a,b,c] The calculated spectra were corrected using scaling factor of 0.964 at B3LYP/6-31+G(d, p) level

B3LPY/6-31+G(d,p)						Assignment[d]	Experimental Spectra	
structure (a)			structure (c)					
ν_{cal}	I_{ir}	I_{Raman}	ν_{cal}	I_{ir}	I_{Raman}		ν_{ir}	ν_{Raman}
404	0.027	0.001	383	0.022	0.006	CF_3 asym bend		
405	0.026	0.001	408	0.024	0.002	CF_3 PF_2 asym bend		
418	0.006	0.002	409	0.005	0.002	CF_3 bend		
420	0.001	0.006	426	0.049	0.002	ring-C bend		
452	0.021	0.002	429	0.001	0.000	P-F asym str	430(0.21)	433(0.10)
453	0.023	0.002	453	0.023	0.004	PC_2 bend	468(0.08)	
494	0.058	0.000	496	0.080	0.000	PF_3 bend	495(0.22)	
502	0.007	0.006	498	0.014	0.006	CF_3 bend		
503	0.006	0.006	506	0.012	0.007	CF_3 bend		
508	0.008	0.012	534	0.047	0.048	CF_3 PF_3 bend	530(0.31)	
558	0.000	0.011	548	0.101	0.006	CF_3 twist		544(0.09)
559	0.000	0.007	559	0.000	0.005	CF_3 twist		
559	0.000	0.005	560	0.002	0.012	CF_3 twist		
576	0.003	0.027	574	0.001	0.027	ring-C str, ring ip deformation		
590	0.055	0.005	584	0.505	0.001	P-F str, CF_2 bend	580(0.40)	
592	0.037	0.004	595	0.062	0.002	CF_2 bend		
599	0.008	0.022	598	0.111	0.041	CF_2 bend		599(0.45)
610	0.012	0.003	610	0.087	0.014	ring op deformation	613(1.00)	
631	0.274	0.004	596	0.047	0.001	P-F str		
639	0.114	0.005	640	0.588	0.012	ring op deformation		637(0.29)
641	0.330	0.003	626	0.084	0.002	PF_2 asym str		
679	0.015	0.013	677	0.016	0.012	ring ip deformation		
682	0.275	0.092	702	0.034	0.074	PF_3 sym str		
710	0.006	0.004	708	0.001	0.000	CF_3 sym str		
711	0.007	0.003	712	0.008	0.026	CF_3 bend		
712	0.055	0.026	717	0.106	0.001	ring HCCH op sym bend	717(0.56)	
715	0.161	0.011	769	0.461	0.002	ring HCCH op sym bend		747(1.00)
781	0.005	0.002	781	0.006	0.001	ethyl CH_2 and CH_3 rock	760(0.25)	
821	0.000	0.006	824	0.000	0.006	ring HCCH op asym bend	806(0.44)	
890	0.040	0.002	894	0.065	0.001	ring-H op bend		
920	0.001	0.004	917	0.170	0.004	PC_3 sym str		
925	0.142	0.003	921	0.164	0.003	C-C str		
925	0.147	0.004	921	0.116	0.004	CF_2 wag		
930	0.009	0.030	929	0.005	0.032	ring-ethyl str	965(0.35)	965(0.15)
1000	0.010	0.051	1002	0.007	0.048	ring HCCH ip bend		
1009	0.007	0.020	1007	0.013	0.027	ring ip deformation		
1054	0.003	0.005	1049	0.023	0.002	CF str		1028(0.28)
1065	0.003	0.029	1066	0.186	0.011	CH_3 twist		
1067	0.087	0.017	1064	0.093	0.011	PF_3 twist		
1068	0.065	0.014	1056	0.020	0.034	C-F str		
1071	0.012	0.005	1072	0.006	0.004	ring-CH3 bend		
1084	0.005	0.028	1083	0.037	0.018	ring HCCH ip bend		
1088	0.078	0.011	1085	0.319	0.042	C-F str		

Table 2 (continued)

B3LYP/6-31+G(d,p)						Assignment[d]	Experimental Spectra	
structure (a)			structure (c)					
ν_{cal}	I_{ir}	I_{Raman}	ν_{cal}	I_{ir}	I_{Raman}		ν_{ir}	ν_{Raman}
1090	0.078	0.012	1098	0.643	0.007	C-F str	1093(0.56)	1093(0.17)
1104	0.009	0.012	1101	0.147	0.027	CH_2 rock, CF_3 twist		
1112	0.795	0.008	1102	0.312	0.004	C-F str		
1115	0.023	0.008	1115	0.031	0.010	CH_3 twist		
1124	0.089	0.022	1119	0.239	0.006	C-F str		
1128	0.094	0.026	1122	0.989	0.027	C-F str	1126(0.67)	
1138	1.000	0.022	1139	0.155	0.021	C-F str		
1153	0.046	0.009	1137	0.661	0.014	ring-H ip bend, HCCH ip rock		
1156	0.070	0.009	1158	0.568	0.002	C-F str		
1164	0.518	0.011	1169	1.000	0.023	C-F str	1167(0.64)	
1167	0.678	0.010	1180	0.770	0.006	C-F str	1183(0.69)	1191(0.10)
1236	0.347	0.023	1241	0.007	0.018	anion C-C str	1210(0.55)	
1237	0.393	0.021	1232	0.497	0.018	anion C-C str		
1239	0.097	0.013	1229	0.378	0.010	ring-ethyl bend		
1261	0.004	0.022	1256	0.237	0.026	anion C-C str		
1279	0.000	0.005	1269	0.000	0.007	ring-ethyl bend, HCCH ip rock		
1303	0.015	0.118	1304	0.023	0.125	ring ip deformation	1301(0.20)	
1339	0.016	0.003	1342	0.026	0.003	CH_2 wag		1336(0.21)
1369	0.002	0.060	1368	0.005	0.069	ring ip deformation, CH_3 sym bend		
1381	0.018	0.018	1380	0.023	0.009	CH_3 sym bend		1390(0.18)
1402	0.011	0.225	1404	0.012	0.252	ring ip deformation		
1415	0.012	0.063	1416	0.017	0.081	CH_3 sym bend	1423(0.34)	
1440	0.026	0.040	1441	0.013	0.101	CH_3 asym bend		
1442	0.008	0.086	1442	0.037	0.037	ethyl bend		
1448	0.019	0.044	1447	0.034	0.052	ethyl bend		
1459	0.021	0.006	1458	0.022	0.003	ethyl bend	1459(0.18)	
1460	0.020	0.097	1461	0.031	0.101	methyl bend		
1549	0.067	0.022	1544	0.128	0.018	ring ip deformation		
1556	0.053	0.027	1554	0.053	0.039	ring ip deformation		
2946	0.027	0.869	2945	0.037	0.915	ethyl CH_3 sym str		
2968	0.030	1.000	2968	0.042	1.000	methyl CH_3 sym str		
2970	0.030	0.768	2978	0.042	0.694	ethyl CH_2 sym str		2982(0.44)
3013	0.021	0.469	3014	0.032	0.498	ethyl CH_3 asym str		
3037	0.003	0.341	3032	0.012	0.356	ethyl asym C-H str		
3046	0.005	0.366	3046	0.008	0.396	methyl CH_3 asym str		
3048	0.005	0.104	3048	0.002	0.120	ethyl CH_2 asym str		
3082	0.009	0.286	3079	0.008	0.264	methyl CH_3 asym str		
3135	0.481	0.525	3169	0.839	0.529	ring-H str		3120(0.10)
3178	0.012	0.278	3176	0.020	0.298	ring HCCH asym str	3183(0.02)	
3195	0.004	0.641	3194	0.001	0.787	ring HCCH sym str		3194(0.20)

[a] The spectra were assigned by visualizing displacements of atoms around their equilibrium positions and via PED (potential energy distribution) analysis. [b] Wavenumbers in unit of cm^{-1}. [c] Both experimental and calculated intensities are normalized by their respective most intense bands. [d] ip: in plane; op: out of plane

density is depleted are weakened. It is important to note that all inter-ionic critical bond points are situated in the purple region where electron density increases.

Interaction energies

Interaction energies were calculated as the difference between the energies of the cation-anion pair and the sum of the energies of the sole cation and anion species,

$$E(\text{int}) = E([\text{Emim}]^+[\text{FAP}]^-) - E([\text{Emim}]^+) - E([\text{FAP}]^-)$$

The counterpoise approach [30] was applied to correct basis-set superposition error (BSSE) [29] and results are shown in Table 1. Comparing to the reported interactions for $[\text{Emim}]^+[\text{PF}_6]^-$ ion pairs which are around 364 kJ/mol [39] (329 kJ/mol at our calculation level, as Table 1 shown), interactions for $[\text{Emim}]^+[\text{FAP}]^-$ ion pairs (around 280 kJ/mol) are much weaker. The weakened interactions are proposed to be important for ILs: they possibly enable more free volume in ILs and result in an enhanced CO_2 capture ability [40].

To investigate the origin of this interaction decrease, Natural Energy Decomposition Analysis (NEDA) [32, 41, 42] were carried out. NEDA identifies interactions into three components: electrical component, core component, and charge transfer component. Electrical component represents the classical-like Coulombic interactions, core component represents repulsions at the equilibrium position which is inside van der Waals contact, and charge transfer represents delocalization interactions between subunits:

$$\Delta E = E(\text{Electrical}) + E(\text{Core}) + E(\text{Charge Transfer})$$

The NEDA results for most stable $[\text{Emim}]^+[\text{FAP}]^-$ conformers are shown in Table 1. As an ionic liquid, it was expected that the electrical components are the largest individual contributors to the total interactions between cation and anion. The charge transfer was shown clearly as another very important component.

Comparing the NEDA results between optimized $[\text{Emim}]^+[\text{PF}_6]^-$ ion pair and $[\text{Emim}]^+[\text{FAP}]^-$ ion paris (Table 1), it suggests that the decrease in interaction energies from $[\text{Emim}]^+[\text{PF}_6]^-$ to $[\text{Emim}]^+[\text{FAP}]^-$ are mainly due to the electrical component. This is reasonable since the distance between cation and anion increases from $[\text{Emim}]^+[\text{PF}_6]^-$ ion pairs to $[\text{Emim}]^+[\text{FAP}]^-$ ion pairs due to bulky $[\text{FAP}]^-$ ion.

Another interaction component which should be investigated is the dispersion term, which is important but not included in DFT calculations. To estimate the dispersion interactions between $[\text{Emim}]^+$ cation and $[\text{FAP}]^-$ anion, the interactions were recalculated at RHF and MP2 levels respectively, and their difference were calculated as dispersion interactions (Table 1). It was shown that comparing to charge transfer or electrical term, dispersion interaction is much weaker for $[\text{Emim}]^+[\text{FAP}]^-$ IL. DFT theory, despite the fact of missing dispersion term, is usually quite successful in predicting accurate structure and vibrational spectra of ILs.

Vibrational spectra and spectral assignments

Harmonic vibrations for most stable $[\text{Emim}]^+[\text{FAP}]^-$ ion pairs were calculated at B3LYP/6-31+G** level and scaled by a factor of 0.964 [43] to compared to experimental Raman and infrared spectra (Fig. 8). The correlation diagram between calculated frequencies and experimental frequencies shows a correlation coeffcient 0.9998 (Fig. 9).

Vibrational peaks were assigned (Table 2) by visualizing displacements of atoms around their equilibrium positions and through Potential Energy Distribution analysis. The most strong peak in the Raman spectrum is located at 748 cm^{-1}. This band is assigned to a ring H-C=C-H symmetric out-of-plane bending. The band region between 2700 and 3200 cm^{-1} is the CH stretching region. Although it was pointed out that the origin of this CH vibrations profile is very complicated [44], they are potential spectroscopic probes for the inter-ionic interactions [45].

Conclusion

In summary, two stable ion pair conformers were predicted using DFT among several other possibilities for the Ionic liquid $[\text{Emim}]^+[\text{FAP}]^-$. $[\text{Emim}]^+$ cation adopts a non-planar orientation and the $[\text{FAP}]^-$ anion adopts both facial and meridional structures in the most stable conformation. Atoms-in-molecules (AIM) analysis indicated the existence of several inter-ionic hydrogen bonds in the ion pair. Interaction energy calculations indicate that $[\text{Emim}]^+[\text{FAP}]^-$ has weaker inter-ionic interactions compared to the $[\text{Emim}]^+[\text{PF}_6]^-$ ion pair. Further, Natural Energy Decomposition Analysis (NEDA) calculations conclude that the decrease in the interaction energy is mainly due to the electrical component, which include both the electrostatic (ES) and polarization (POL) contributions. Assignments of the experimental and computed IR and Raman spectra were done by visualizing displacement of atoms around their equilibrium positions and through Potential Energy Distribution (PED) analysis.

Acknowledgments This technical effort was performed in support of the National Energy Technology Laboratorys ongoing research in CO_2 Capture under the RES contract DE-FE0004000.

References

1. Holbrey JD, Seddon KR (1999) Clean Techn Environ Policy 1:223. doi:10.1007/s100980050036
2. Welton T (1999) Chem Rev 99:2071. doi:10.1021/cr980032t
3. Earle MJ, Seddon KR. (2000) Pure Appl Chem 72:1391. doi:10.1351/pac200072071391
4. Wasserscheid P, Keim W (2000) Angewandte Chemie, Int Ed 39:3772. doi:10.1002/1521-3773(20001103)
5. Lagrost C, Carrié D, Vaultier M, Hapiot P (2003) J Phys Chem A 107:745. doi:10.1021/jp026907w
6. Bates ED, Mayton RD, Ntai I, Davis JH (2002) J Am Chem Soc 124:926. doi:10.1021/ja017593d
7. Lim BH, Choe WH, Shim JJ, Ra CS, Tuma D, Lee H, Lee CS (2009) Korean J Chem Eng 26:1130. doi:10.1007/s11814-009-0188-5
8. Smiglak M, Metlen A, Rogers RD (2007) Acc Chem Res 40:1182. doi:10.1021/ar7001304
9. Mao Y, Damodaran K (2014) Chem Phys 440:87. doi:10.1016/j.chemphys.2014.06.014
10. Ignatev N, Welz-Biermann U, Kucheryna A, Bissky G, Willner H (2005) J Fluor Chem 126:1150. doi:10.1016/j.jfluchem.2005.04.017
11. Yao C, Pitner WR, Anderson JL (2009) Anal Chem 81:5054
12. Marciniak A, Wlazo M (2010) J Phys Chem B 114:6990
13. Gonzalez R, Battez AH, Blanco D, Viesca JL, Fernandez-Gonzalez A (2010) Tribol Lett 40:269
14. Li H, Rutland MW, Atkin R (2013) Phys Chem Chem Phys 15:14616. doi:10.1039/C3CP52638K
15. Blanco D, Gonzaleza R, Battez AH, Viesca JL, FernAdez-Gonzalezb A (2011) Tribol Int 44:645
16. Blanco D, Battez AH, Viesca JL, Gonzalez R, Fernandez-Gonzalez A (2011) Tribol Lett 41:295
17. Druschler M, Huber B, Roling B (2011) J Phys Chem C 115:6802
18. Zhang X, Liu Z, Wang W (2008) AIChE J 54:2717
19. Zhang X, Huo F, Liu Z, Wang W, Shi W, Maginn EJ (2009) J Phys Chem B 113:7591. doi:10.1021/jp900403q
20. Althuluth M, Mota-Martinez MT, Kroon MC, Peters CJ (2012) J Chem Eng Data 57:3422. doi:10.1021/je300521y
21. Mao JX, Nulwala HB, Luebke DR, Damodaran K (2013) J Mol Liq 175:141. doi:10.1016/j.molliq.2012.09.001
22. Mao JX, Lee AS, Kitchin JR, Nulwala HB, Luebke DR, Damodaran K (2013) J Mol Struct 1038:12. doi:10.1016/j.molstruc.2013.01.046
23. Allen JJ, Bowser SR, Damodaran K (2014) Phys Chem Chem Phys 16:8078. doi:10.1039/c3cp55384a
24. Althuluth M, Berrouk A, Kroon MC, Peters CJ (2014) Ind Eng Chem Res 53:11818. doi:10.1021/ie5003729
25. Becke AD (1993) J Chem Phys 98:5648. doi:10.1063/1.464913
26. Lee C, Yang W, Parr RG (1988) Phys Rev B: Condens Matter Mater Phys 37:785. doi:10.1103/PhysRevB.37.785
27. Frisch MJ, Trucks GW, Schlegel HB, Scuseria GE, Robb MA, Cheeseman JR, Scalmani G, Barone V, Mennucci B, Petersson GA, Nakatsuji H, Caricato M, Li X, Hratchian HP, Izmaylov AF, Bloino J, Zheng G, Sonnenberg JL, Hada M, Ehara M, Toyota K, Fukuda R, Hasegawa J, Ishida M, Nakajima T, Honda Y, Kitao O, Nakai H, Vreven T, Montgomery JA Jr., Peralta JE, Ogliaro F, Bearpark M, Heyd JJ, Brothers E, Kudin KN, Staroverov VN, Kobayashi R, Normand J, Raghavachari K, Rendell A, Burant JC, Iyengar SS, Tomasi J, Cossi M, Rega N, Millam JM, Klene M, Knox JE, Cross JB, Bakken V, Adamo C, Jaramillo J, Gomperts R, Stratmann RE, Yazyev O, Austin AJ, Cammi R, Pomelli C, Ochterski JW, Martin RL, Morokuma K, Zakrzewski VG, Voth GA, Salvador P, Dannenberg JJ, Dapprich S, Daniels AD, Farkas, Foresman JB, Ortiz JV, Cioslowski J, Fox DJ (2009) Gaussian 09 Revision A.1. Gaussian Inc. Wallingford CT 2009
28. Frisch MJ, Pople JA, Binkley JS (1984) J Chem Phys 80:3265. doi:10.1063/1.447079
29. Jansen HB, Ros P (1969) Chem Phys Lett 3:140. doi:10.1016/0009-2614(69)80118-1
30. Boys SF, Bernardi F (1970) Mol Phys 19:553. doi:10.1080/00268977000101561
31. Szczesniak MM, Scheiner S (1986) J Chem Phys 84:6328. doi:10.1063/1.450725
32. Glendening ED, Streitwieser A (1994) J Chem Phys 100:2900. doi:10.1063/1.466432
33. Koch U, Popelier PLA (1995) J Phys Chem 99:9747. doi:10.1021/j100024a016
34. Popelier PLA (1998) J Phys Chem A 102:1873. doi:10.1021/jp9805048
35. Granovsky AA Firefly, version 8.0.0 rc. http://www.classic.chem.msu.su/gran/firefly/index.html
36. Turner EA, Pye CC, Singer RD (2003) J Phys Chem A 107:2277. doi:10.1021/jp021694w
37. Umebayashi Y, Fujimori T, Sukizaki T, Asada M, Fujii K, Kanzaki, R, ichi Ishiguro S (2005) J Phys Chem A 109:8976. doi:10.1021/jp053476j
38. Bader RFW (1991) Chem Rev 91:893. doi:10.1021/cr00005a013
39. Tsuzuki S, Tokuda H, Hayamizu K, Watanabe M (2005) J Phys Chem B 109:16474. doi:10.1021/jp0533628
40. Mahurin SM, Lee JS, Baker GA, Luo H, Dai S (2010) J Membr Sci 353:177. doi:10.1016/j.memsci.2010.02.045
41. Schenter GK, Glendening ED (1996) J Phys Chem 100:17152. doi:10.1021/jp9612994
42. Glendening ED (1996) J Am Chem Soc 118:2473. doi:10.1021/ja951834y
43. Nist computational chemistry comparison and benchmark database, nist standard reference database number 101 (2013) Release 16a, August 2013, Russell D. Johnson III (ed), http://cccbdb.nist.gov
44. Buffeteau T, Grondin J, Lassègues JC (2010) Appl Spectrosc 64:112. doi:10.1366/000370210790572089
45. Talaty ER, Raja S, Storhaug VJ, Dölle A, Carper WR (2004) J Phys Chem B 108:13177. doi:10.1021/jp040199s